Fourier optics modelling of instrument response for interference microscopy

de Groot, Peter, Colonna de Lega, Xavier

SPIE.

Fourier optics modelling of instrument response for interference microscopy

Peter de Groot and Xavier Colonna de Lega

Zygo Corporation, Laurel Brook Road, Middlefield, CT 06455

ABSTRACT

Interferometers for the measurement of topography rely on imaging systems to map surface points to a camera. The response of an interferometer to variations in surface height depends on the filtering properties of the imaging system. Here we provide a simple and practical model of an imaging interferometer using classical Fourier optics, including the effects of partial coherence. The model is useful for understanding basic properties such as lateral resolution and error sources related to measurement principles that make assumptions regarding the fidelity of the instrument response over a range of surface spatial frequencies and light source wavelengths.

Keywords: Interferometry, diffraction, interference, instrument transfer function, optical transfer function, metrology

1. INTRODUCTION

The modelling of interference microscopes has advanced considerably, providing details of the interaction of light with complex surface structures, multiple scattering, the effect of semi-transparent surface films and optically unresolved structures. These advances have provided important insight into instrument behavior, particularly for difficult surface structures that can generate unexpected or anomalous results [1-3]. These methods rely on rigorous solutions to Maxwell's equations, often combined with 3D transfer functions, to provide insights into the combined effects of focus and light source bandwidth on interference signals [4, 5].

The benefits of advanced modeling notwithstanding, fundamental Fourier optics and classical Abbe theory continue to play important roles in understanding interferometers for surface topography measurement [6-8]. These traditional methods are accessible to most researchers with a basic understanding of Fourier optics, and provide an intuitive path to understanding the limits of lateral resolution and the origins of measurement errors, particularly with multiple-wavelength and coherence-based interference techniques. Consequently, somewhat contrary to current trends that strive to improve diffraction calculations on difficult surface structures, the goal of the present research is to provide the simplest possible interferometer model that realistically includes the imaging properties of the optical system. We refer to this approach as the elementary Fourier optics (EFO) model.

A specific case of interest here is interferometry with partially coherent light, which is common in reflection interference microscopes for surface topography measurement. Modeling partially coherent systems usually involves an integration over a grid of points in the illumination pupil representing an extended light source [9]. In addition to being computationally intensive, it is difficult to interpret the pupil plane integration in terms of familiar concepts such as the modulation transfer function for optical imaging. However, we have recently shown that using the EFO model with familiar approximations such as an obliquity factor for fringe spacing simplifies the integration to a simple linear filtering with a 2D (x, y) transfer functions [10]. This approach provided an intuitive way of understanding and predicting basic instrument response in interferometers, with clear limitations given the approximations involved. The model is useful for understanding basic properties such as lateral resolution and error sources related to measurement principles that make assumptions regarding the fidelity of the instrument response over a range of surface spatial frequencies and light source wavelengths.

In this paper, we first describe in section 2 a generic imaging interferometer, and summarize in section 3 the approximate partially-coherent EFO model from Ref.[10]. An example in section 4 of a simulated sinusoidal grating clarifies the sequence of operations leading to a calculation of the predicted measured profile. Section 5 includes a calculation of the topographical image of two features spaced by the Rayleigh resolution limit. As an example of the extensibility of the model, section 6 provides a cross-sectional image of wave propagation over a range of focus positions. Following this example is a summary and outlook for further work.

2. INSTRUMENT

Figure 1 shows a simple generic hardware model of an interferometer that includes an imaging system [11]. The objective lens has an imaging numerical aperture (NA) A_N determined by its focal length and the objective aperture stop that in the model is positioned at the back focal plane of the objective lens. The reference and object lenses have the same NA, consistent with the most common microscope configurations. The monochromatic Köhler illumination images the light source into the back focal plane. Depending on the aperture, the illumination NA A_P is less than or equal to the imaging NA A_N. For a point-like monochromatic light source such as a laser or a very small aperture stop such that $A_P \ll A_N$, the illumination is spatially coherent; whereas if the light source is diffuse and its image fills the objective aperture, $A_P = A_N$ and the illumination is nearly incoherent.
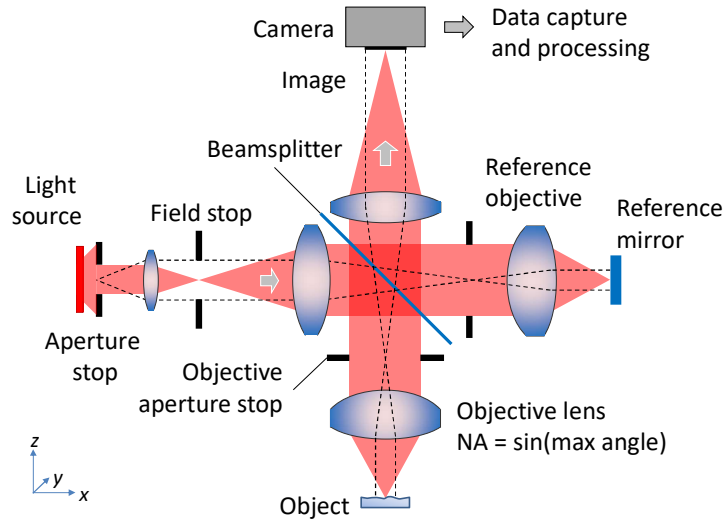
Figure 1: Hardware model of an interference microscope.

In EFO modeling, the basic assumption is that variations in surface height are small when compared to the depth of field given by the Rayleigh formula

$$D_{field} = \pm \lambda / A_N^2 . \tag{1}$$

For a wavelength of 0.50 μm, the depth of field typically ranges from ±100 μm at 0.05 NA to ±1 μm at 0.5 NA. This is range of surface heights accommodates a wide range of practical situations, including coherence-scanning methods, if we consider only those areas within the field of view that are in focus during the scan [12].

This paper assumes several additional common approximations, including neglecting angle-dependent reflectivity variations, polarization effects and skew angles. As noted in the Introduction, a further simplification for partially coherent light follows from the use of the obliquity factor—a familiar concept in interference microscopy that averages the interference phase shift sensitivity over the range of incident angles to the object surface. The obliquity factor significantly simplifies the calculation, enabling the use of Fourier transforms and familiar methods of linear transfer functions [10].

3. MATHEMATICAL MODEL

The camera in Figure 1 detects an interference signal

$$\Upsilon = \left(\Upsilon_R + \Upsilon_I \right) + \Upsilon_{IR} , \tag{2}$$

where Υ_R, Υ_I correspond to individual contributions from the imaged reference and object light, respectively, and Υ_{IR} is the interference term. In this paper, we are only interested in the interference term Υ_{IR}. The interference term by definition is given by

$$\Upsilon_{IR} = U_R^* \, U_I + U_R \, U_I^*, \tag{3}$$

where U_R, U_I are complex representations of the contributions to the interference effect from the reference and object surface reflections, respectively, including the effects of the imaging optics. A simple model of the reference, assuming that there is no field dependence for the magnitude $|U_R|$ nor for the phase θ_R, is

$$U_R = \exp(-i\theta_R). \tag{4}$$

Although mathematically the quantities U_R, U_I are defined as interference contributions, they may be thought of informally as imaged light fields in the EFO model. This concept is to be used with caution, as these variables are the result of a sequence of mathematical approximations and do not directly represent the imaged light fields from the object and reference independent of the interference calculation [10]. For example, the non-interfering term Υ_I in partially coherent light is not equal to the square magnitude $|U_I|^2$, except for the limit case of fully coherent imaging with a point-like source [13, 14]. This is the reason for using non-italic symbols for U_R, U_I, consistent with previous papers [10].

The calculation of the object contribution U_I begins with the definition of a surface height profile $h_o(x)$ along a surface coordinate x, which serves as an abbreviation for the two-dimensional lateral coordinates x, y. The instrument illuminates the surface with monochromatic light having an angular wavenumber

$$k = 2\pi/\lambda. \tag{5}$$

In the model, the effect of topography is to introduce phase shifts proportional to surface heights $h_o(x)$:

$$\theta_{eq}(x) = 2k_{eq} h_o(x) \tag{6}$$

where the *obliquity factor* defined by

$$\Omega = k/k_{eq} \tag{7}$$

accounts for the average increase in interference fringe spacing with oblique illumination over a range of incident angles [11, 15, 16]. A known formula for the obliquity factor for a uniform, disk-shaped source light distribution within the illumination pupil for low NA (<0.5) is

$$\Omega = 2/[1 + \cos(\beta_P)], \tag{8}$$

where β_P is the maximum incident angle for the illumination cone, given by

$$\beta_P = \sin^{-1}(A_P). \tag{9}$$

A complex distribution $U_o(x)$ within a plane at $z = 0$ represents the effect of the object surface on the light reflected from the object surface:

$$U_o(x) = \exp\left[-i\theta_{eq}(x)\right] . \tag{10}$$

Following conventional methods of Fourier optics, this distribution is represented by a spectrum of plane waves

$$\widetilde{U_o}(f_x) = \int U_o(x)\exp(-i2\pi f_x x)\, df_x . \tag{11}$$

The tilde (~) symbol denotes a frequency-domain representation of the corresponding space-domain quantity. The lateral spatial frequency f_x for each plane wave follows from the grating equation

$$\cos(\alpha_x) = \lambda f_x , \tag{12}$$

where α_x is the angle between the direction of the plane wave propagation and the x axis. The inverse Fourier transform provides the resulting light field from the focus-shifted spectrum of plane waves.

The modeling of image formation includes the filtering properties of the optical system. In the simplest EFO model, the use of an obliquity factor allows us to perform the filtering on the complex amplitude $\widetilde{U_o}$, as if the system were fully coherent. The effect on the spectrum of plane waves is a multiplication in frequency space

$$\widetilde{U_I}(f_x) = \widetilde{O}(f_x)\widetilde{U_o}(f_x), \tag{13}$$

where the partially-coherent transfer function (PCTF)

$$\widetilde{O}(f_x) = \left[\widetilde{P}(f_x)\widetilde{H}(f_x)\right] \star \widetilde{H}(f_x), \tag{14}$$

is a cross-correlation involving the classical amplitude transfer function (ATF) $\widetilde{H}(f_x)$, and $\widetilde{P}(f_x)$ is the light source intensity distribution within the illumination pupil. The PCTF determines the frequency bandwidth of the instrument response as well as the effects of aberrations.

In the simplest case of an optical design considered free of all aberrations, a uniform source distribution limited by an illumination aperture and the ATF limited by an imaging aperture, we have

$$\widetilde{H}(f_x) = \operatorname{circ}\{f_x/f_N\} \tag{15}$$

$$\widetilde{P}(f_x) = \operatorname{circ}\{f_x/f_P\} \tag{16}$$

where the limiting spatial frequencies are

$$f_N = A_N/\lambda \tag{17}$$

$$f_P = q\, f_N \tag{18}$$

and the *fill factor* $q \leq 1$ is equal to the ratio of the diameter of the circular source light image in the illumination pupil to the diameter of the illumination aperture. The PCTF works out to

$$\widetilde{O}(f_x) = \begin{cases} 0 & \text{if } |f_x| > f_N + f_P \; , \quad \text{otherwise} \\ 1 & \text{if } |f_x| \leq f_N - f_P \; , \quad \text{otherwise} \\ \dfrac{1}{\pi}\dfrac{f_N^2}{f_P^2}\big[\beta_N - \cos(\beta_N)\sin(\beta_N)\big] + \dfrac{1}{\pi}\big[\beta_P - \cos(\beta_P)\sin(\beta_P)\big] \end{cases} \tag{19}$$

where

$$\begin{aligned} \cos(\beta_N) &= \frac{|f_x|}{2f_N} + \frac{f_N^2 - f_P^2}{2f_N}\frac{1}{|f_x|} \\ \cos(\beta_P) &= \frac{|f_x|}{2f_P} - \frac{f_N^2 - f_P^2}{2f_P}\frac{1}{|f_x|} \; . \end{aligned} \tag{20}$$

This result covers all cases from a point source with $A_P \ll A_N$ to a filled pupil $A_P = A_N$. For the case of a filled pupil, the result is identical to the well-known MTF formula for a conventional fully-incoherent imaging system [17]. For the case of an overfilled pupil such that $q > 1$, the imaging aperture A_N limits the lateral resolution just as it does in conventional microscopy with a condensing lens, and the PCTF is calculated for $q = 1$.

At the image plane, the coherent superposition of the filtered plane waves results in an imaged light field given by the inverse Fourier transform

$$U_I(x) = \int \widetilde{U_I}(f_x)\exp(i2\pi f_x x)\,df_x , \tag{21}$$

where we have reused the object-space coordinates x, z, equivalent to a system without distortion and with unit magnification. The calculation of the topography follows from a determination of the phase of the imaged light field, ideally at the best focus position.

$$\theta_I(x) = -\arg\{U_I(x)\} . \tag{22}$$

The topography measurement is

$$h_I(x) = \theta_I(x)/2k_{eq} = \Omega\lambda\theta_I(x)/4\pi . \tag{23}$$

Because the phase range covers only 2π, the measured value should be unwrapped or connected to cover the full topography range in the usual way. In practice, determining the phase interferometrically may proceed by any one of a number of ways, for example, by mixing the imaged light field with the reference field and performing phase shifts to generate a signal for further processing [18]. However, for the purposes of mathematically modeling the effect of surface topography, it is enough to calculate the phase directly from Eq.(22). Table 1 summarizes the approximate EFO interferometer model for partially coherent monochromatic illumination.

Table 1: Approximate EFO model for partially coherent light

Step	Symbols
Determine the obliquity factor and equivalent wavenumber based on the light distribution in the illumination pupil	Ω, k_{eq}
Define an object topography and equivalent phase for the object light field after reflection from the surface	h_o, θ_{eq}
Calculate the complex representation of the object light field and use a Fourier transform to obtain the spectrum of plane waves	U_o, $\widetilde{\mathrm{U}}_o$
Define the light intensity distribution in the illumination pupil and the ATF for the imaging optics	$\widetilde{P}$, $\widetilde{H}$
Calculate the PCTF	$\widetilde{O}$
Filter the spectrum of plane waves using the PCTF, and calculate the imaged light field using an inverse Fourier transform	$\widetilde{\mathrm{U}}_I$, U_I
Calculate the measured phase and corresponding surface heights	θ_I, h_I

4. EXAMPLE: SINUSOIDAL SURFACE TOPOGRAPHY

For a sinusoidal topography object of amplitude b_o and surface spatial frequency v the surface height variation is

$$h_o(x) = b_o \cos(2\pi v x). \tag{24}$$

The corresponding phase shift is

$$\theta_o(x) = 2k_{eq}b_o \cos(2\pi v x). \tag{25}$$

As a specific example, we will use the following parameters

$$
\begin{aligned}
v &= 1/(10\,\mu\text{m}) \\
\lambda &= 500\,\text{nm} \\
b_o &= 0.06\,\mu\text{m} \\
A_N &= 0.100 \\
A_P &= 0.075
\end{aligned}
\tag{26}
$$

Figure 2 is a cross-section of the topography. Figure 3 shows the resulting Fourier spectrum from Eq.(11), while Figure 4 shows the PCTF for the parameters of Eq.(26). After applying this PCTF, we have the truncated spectrum shown in Figure 5. Figure 6 compares the resulting measured surface profile with the original, showing a modest attenuation. Importantly, the optical filtering results in a distortion of the measured surface profile, such that the result is no longer perfectly sinusoidal. This is illustrated by the graph of the predicted measurement error in Figure 7. The distortion in this case is small; but is nonetheless evidence of a nonlinear response that has been a topic of many studies.

Curiosity at least suggests a comparison with an alternative theoretical framework to determine if the nonlinearities shown in Figure 7 are simply the result of over-simplification. Figure 8 shows the difference in the predicted measured profile for the EFO model and a more sophisticated diffraction calculation published by Maystre, et al. adapted for 5-frame phase shifting interferometry [19]. The RMS difference of 0.25 nm provides confidence that at least for simple structures at low NA, the EFO results are consistent with more advanced methods.
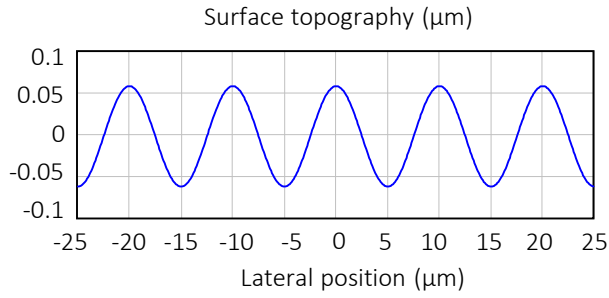
Figure 2: Example sinusoidal topography.
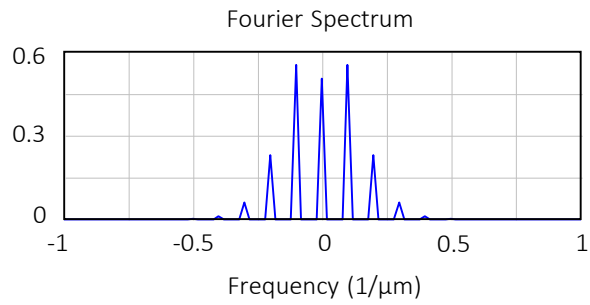
Figure 3: Fourier spectrum for the object contribution to the interference pattern.
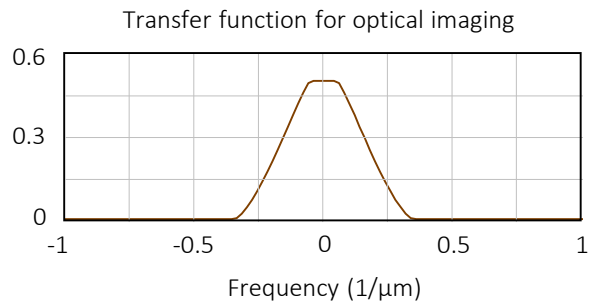
Figure 4: Transfer function representing optical filtering in the frequency domain.
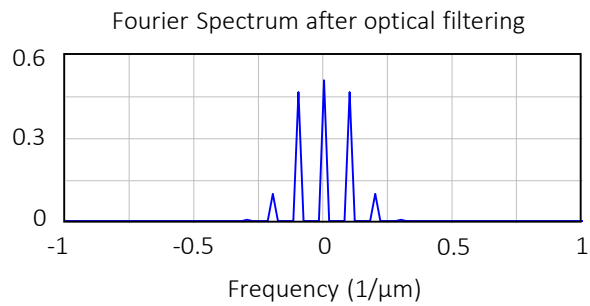
Figure 5: Filtered spectrum after applying the PCTF of Figure 4.
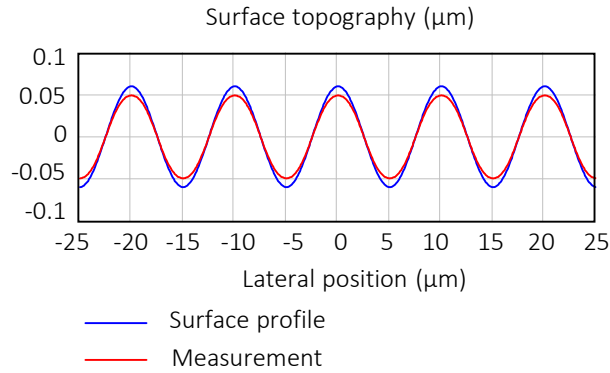
Figure 6: Comparison of the predicted measured surface topography with the known topography.
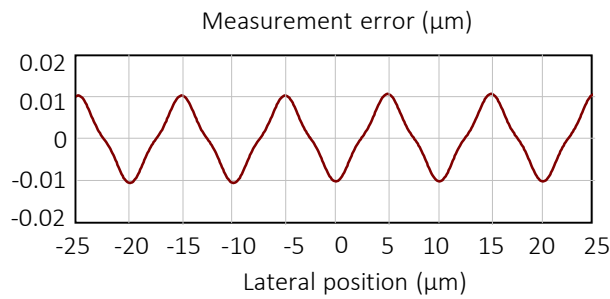
Figure 7: Predicted difference between the measured and known object surface topography.
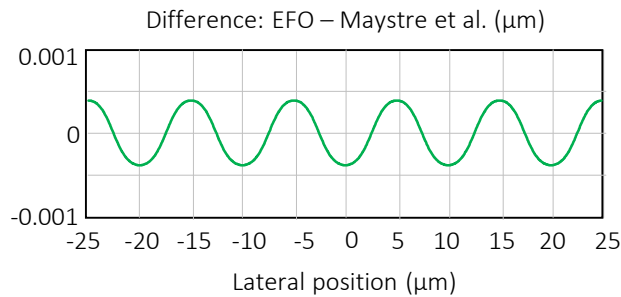
Figure 8: Difference between the predicted measured profiles for the EFO model and the more advanced Maystre et al. model.

5. EXAMPLE: LATERAL RESOLUTION

It is common to specify the resolving power of interferometers according to the traditional Rayleigh or Sparrow limits, which are applicable for intensity variations. It is not so obvious that the same limits apply to surface topography. This is straightforward to test with the approximate EFO model for feature heights that are small compared to the depth of field.

The Rayleigh limit for a disk pupil that is entirely filled with source light is

$$x_{lim} = 0.61 \lambda / A_N \,. \tag{27}$$

The following example parameters make the calculation simple:

$$\lambda = 600\ \text{nm}$$
$$A_N = 0.061$$
$$A_P = 0.061$$
$$x_{lim} = 6\ \mu\text{m}$$

(28)

Figure 9 illustrates the calculation for two lines (posts in cross section) with a 40 nm height and 1 µm width separated by the Rayleigh limit of 6 µm. The features are clearly separable; but there is a significant reduction in surface height to about 20% of the original value. This effect is analogous to the loss of contrast between bright and dark lines in a conventional imaging system.

Surface topography (µm)   Measured topography (µm)
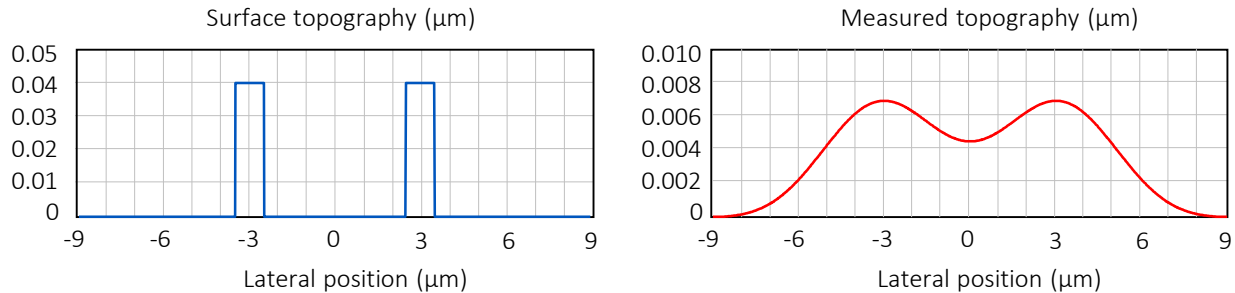
Figure 9: (Left) Object topography for two 40 nm tall features separated by the Rayleigh criterion.
(Right) Simulated measured topography for an interferometer.

The results change with topography features of larger height, but not necessarily in an expected way. As the heights increase, the two features remain properly resolved; but the attenuation of the measured heights is proportionally greater. This is a consequence of more light being scattered at higher angles by taller structures, resulting in light loss at the limiting apertures of the system. The effect is illustrated in Figure 10 for a feature height of 120 nm. Note that when comparing Figure 10 with Figure 9, the relative scales between the left and right graphs have been preserved. The conclusion is that for these narrow, closely-spaced rectangular features, the instrument response is nonlinear; but the system is still able to resolve feature separations consistent with the Rayleigh criterion.

Surface topography (µm)   Measured topography (µm)
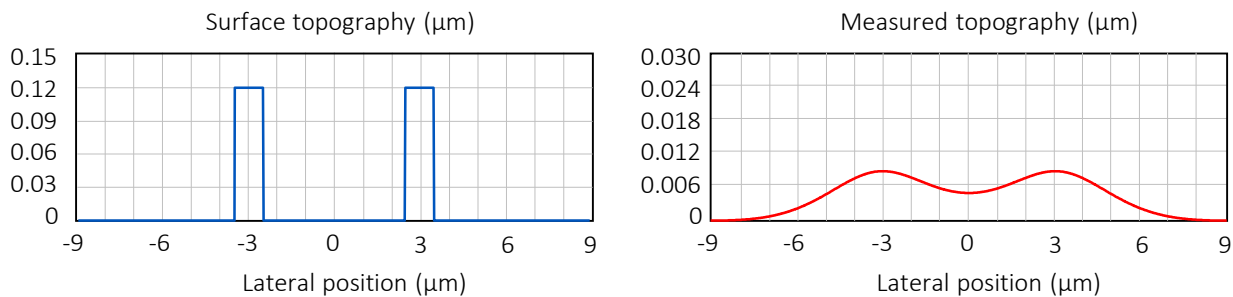
Figure 10: (Left) Object topography for two 120 nm tall features separated by the Rayleigh criterion.
(Right) Simulated measured topography.

6. FOCUS EFFECTS

The EFO model assumes that the variations in surface height for the object surface should be less than the depth of field of the instrument. However, this does not mean that the surface as a whole must be at the best-focus position. With this understanding, it is straightforward to include an image focus change along the z axis using traditional Fourier optics methods. The free-space propagator

$$\wp(f_x, z) = \exp\left[ikz\sqrt{1 - (\lambda f_x)^2}\right] \tag{29}$$

accounts for how much each plane wave will be shifted in phase in terms of a propagation distance z

$$\widetilde{U_o}(f_x, z) = \wp(f_x, z)\widetilde{U_o}(f_x). \tag{30}$$

The square root in the propagator implies that we retain only those non-evanescent plane waves for which $\lambda f_x \le 1$. The inverse Fourier transform is the focus-shifted object light field:

$$U_o(x, z) = \int \widetilde{U_o}(f_x, z)\exp(i2\pi f_x x)\, df_x \tag{31}$$

In addition to image defocus, as the object moves away from this position, there is a loss of interference fringe contrast in partially coherent illumination caused by the angular dependence of the phase shifts of the component incident beams with z position. This effect is neglected in the approximate EFO model using the obliquity factor. However, Schulz [15] and later Dubois [16] have shown that it is possible to extend the useful focus range for an obliquity factor approximation using a closed-form fringe contrast function as an overall multiplicative factor.

Figure 11 shows an example of the effect of defocus using the propagator of Eq.(29), illustrating the superposition of 500 nm monochromatic diffracted plane waves for a sinusoidal structure having a surface spatial period of 2.5 μm, an amplitude of 0.125 μm, and a width of a 7.5 μm. The image shows the results of the calculation of the defocused light field in Eq.(31) over a 100 μm range of focus positions. The spectrum of plane waves evolves in the far field (upper part of the figure) to a range diffracted orders; whereas in the near field (lower part of the figure) the brightness shows the variation in signal strength across the 7.5 μm surface topography in the vicinity of best focus.
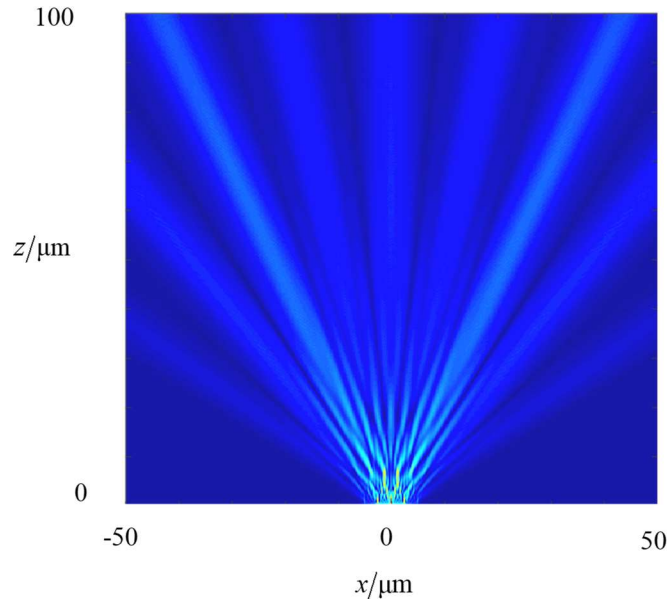
Figure 11: Illustration of the modeling of defocus in the EFO model for a sinusoidal surface topography. The brightness in the image is proportional to the interference signal strength. The in-focus image is at the z=0 position.

7. SUMMARY

In this paper we propose that the basic imaging properties of optical systems can be meaningfully addressed with traditional Fourier optics, using a scattering model that considers the surface as a thin phase grating and a 2D representation of propagating light fields. Within well-recognized limits and with simple surface structures, the model can be useful for predicting interferometer response to sample topography.

In the approximate EFO model summarized in Table 1, a further simplification for partially coherent monochromatic light follows from the use of the obliquity factor—a familiar concept in interference microscopy that averages the interference phase shift sensitivity over the range of incident angles to the object surface. As we have shown in previous work [10], subject to significant limitations related to several approximations, the interference signal can be simulated by assuming that the light source is fully coherent, even if it is an extended source such as a quasi-monochromatic LED. A linear shift-invariant transfer function—the PCTF—accounts for the optics and the process of forming interference fringes on the camera. This approach leverages simple 2D Fourier transforms and is correspondingly easier to implement than a formal pupil-plane integration. The EFO model is simple enough that it can be implemented as in Microsoft® EXCEL® for surface profiles using only standard spreadsheet formulas. An example implementation is available for download from zygo.com [20] and from researchgate.com [21].

The model readily extends to a variety of interferometer configurations and measurement principles, from laser Fizeau systems to coherence scanning interferometry. Although there are clear limitations to such elementary methods, the EFO model can be a first step in understanding many of the most important properties of interferometers, including limits to lateral resolution and many basic error mechanisms observed in practice [14]. In addition, when developing more advanced models, EFO methods are useful for comparison, particularly when elementary methods are proven to be inaccurate, as this indicates situations where evaluation and improvement of topographical fidelity require a more advanced approach.

8. ACKNOWLEDGEMENTS

REFERENCES

[1]   de Groot, P., Colonna de Lega, X., Liesener, J., and Darwin, M., "Metrology of optically-unresolved features using interferometric surface profiling and rcwa modeling," Optics Express 16(6), 3970 (2008).

[2]   Thomas, M., Su, R., Nikolaev, N., Coupland, J., and Leach, R., "Modelling of coherence scanning interferometry for complex surfaces based on a boundary element method," Proc. SPIE 11057 (2019).

[3]   Xie, W., Hagemeier, S., Bischoff, J., Mastylo, R., Manske, E., and Lehmann, P., "Transfer characteristics of optical profilers with respect to rectangular edge and step height measurement," 10329, 16 (2017).

[4]   Coupland, J. M., and Lobera, J., "Holography, tomography and 3d microscopy as linear filtering operations," Measurement Science and Technology 19(7), 074012-1 - 074012-12 (2008).

[5]   Su, R., Thomas, M., Liu, M., Coupland, J., and Leach, R., "High-accuracy surface measurement through modelling of the surface transfer function in interference microscopy," Proc. SPIE 11102, 1110205-1-6 (2019).

[6]   Duffieux, P. M., [L'integrale de fourier et ses applications a l'optique], Imprimeries Oberthur, Rennes (1946).

[7]   Hopkins, H. H., "On the diffraction theory of optical images," Proc. Royal Society A 217, 408-432 (1953).

[8]   Church, E., and Takacs, P., [Effects of the optical transfer function in surface profile measurements], SPIE, OP (1989).

[9]   Totzeck, M., "Numerical simulation of high-na quantitative polarization microscopy and corresponding near-fields," Optik - International Journal for Light and Electron Optics 112(9), 399-406 (2001).

[10]   de Groot, P., and Colonna de Lega, X., "Fourier optics modeling of interference microscopes," J. Opt. Soc. Am. A 37(9), B1-B10 (2020).

[11]   de Groot, P. J. "Interference microscopy for surface structure analysis," [Handbook of optical metrology], T. Yoshizawa, Ed., CRC Press, 31 (2015).

[12]   de Groot, P., "Principles of interference microscopy for the measurement of surface topography," Advances in Optics and Photonics 7(1), 1-65 (2015).

[13]   De, M., and Mondal, P. K., "Phase and amplitude contrast microscopy in partially coherent light," Journal of Research of the National Bureau of Standards-C. Engineering and Instrumentation 69C(3), (1965).

[14]   Ichioka, Y., and Suzuki, T., "Image of a periodic complex object in an optical system under partially coherent illumination," Journal of the Optical Society of America 66(9), 921-932 (1976).

[15]   Schulz, G., "Über interferenzen gleicher dicke und längenmessung mit lichtwellen," Annalen der Physik 449(3-5), 177-187 (1954).

[16]   Dubois, A., Selb, J., Vabre, L., and Boccara, A.-C., "Phase measurements with wide-aperture interferometers,"
         Applied Optics 39(14), 2326 (2000).
[17]   Boreman, G. D., [Modulation transfer function in optical and electro-optical systems], SPIE Press, Bellingham
         (2001).
[18]   Schreiber, H., and Bruning, J. H. "Phase shifting interferometry," [Optical shop testing], D. Malacara, Ed., John
         Wiley & Sons, Inc., (2006).
[19]   Maystre, D., Mendez, O. M., and Roger, A., "A new electromagnetic theory for scattering from shallow rough
         surfaces," Optica Acta: International Journal of Optics 30(12), 1707-1723 (1983).
[20]   https://www.zygo.com/library/papers/Fourier-Optics-Interferometry-Demonstrator.xlsx
[21]   https://www.researchgate.net/publication/343362887_Fourier_Optics_interferometry_demonstrator